arXiv:2207.13532v2 [cs.CV] 28 Nov 2022

Contrastive Masked Autoencoders are Stronger Vision Learners

Zhicheng Huang[1*] **Xiaojie Jin**[2†] **Chengze Lu**[3*] **Qibin Hou**[3]
Ming-Ming Cheng[3] **Dongmei Fu**[1] **Xiaohui Shen**[2] **Jiashi Feng**[2†]
[1] University of Science and Technology Beijing [2] Bytedance Inc. [3] Nankai University

Abstract

Masked image modeling (MIM) has achieved promising results on various vision tasks. However, the limited discriminability of learned representation manifests there is still plenty to go for making a stronger vision learner. Towards this goal, we propose Contrastive Masked Autoencoders (CMAE), a new self-supervised pre-training method for learning more comprehensive and capable vision representations. By elaboratively unifying contrastive learning (CL) and masked image model (MIM) through novel designs, CMAE leverages their respective advantages and learns representations with both strong instance discriminability and local perceptibility. Specifically, CMAE consists of two branches where the online branch is an asymmetric encoder-decoder and the target branch is a momentum updated encoder. During training, the online encoder reconstructs original images from latent representations of masked images to learn holistic features. The target encoder, fed with the full images, enhances the feature discriminability via contrastive learning with its online counterpart. To make CL compatible with MIM, CMAE introduces two new components, i.e. pixel shifting for generating plausible positive views and feature decoder for complementing features of contrastive pairs. Thanks to these novel designs, CMAE effectively improves the representation quality and transfer performance over its MIM counterpart. CMAE achieves the state-of-the-art performance on highly competitive benchmarks of image classification, semantic segmentation and object detection. Notably, CMAE-Base achieves 85.3% top-1 accuracy on ImageNet and 52.5% mIoU on ADE20k, surpassing previous best results by 0.7% and 1.8% respectively. Codes will be made publicly available at https://github.com/ZhichengHuang/CMAE.

1 Introduction

Masked image modeling (MIM) [19, 25, 43] has been attracting increasing attention recently in the self-supervised learning field, due to its method simplicity and capability of learning rich and holistic representations. Following the idea of masked language modeling in NLP [15], they randomly mask a large portion of the training image patches and use an auto-encoder [26] to reconstruct the original signals (e.g., raw pixels, offline extracted features) of the masked patches. It has been shown in [19, 25, 43] that such a simple framework outperforms previous self-supervised learning methods in both ImageNet classification [14] and some downstream tasks, like object detection and semantic segmentation.

*Work done when Zhicheng Huang and Chengze Lu interned at Bytedance Inc.
†Corresponding author: Xiaojie Jin<jinxiaojie@bytedance.com>, Jiashi Feng<jshfeng@bytedance.com>.

Preprint. Under review.

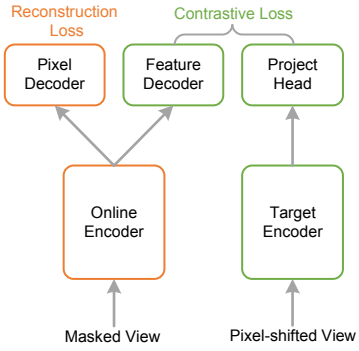

Figure 1: Overview of CMAE. CMAE improves over its MIM counterpart by leveraging contrastive learning through novel designs.

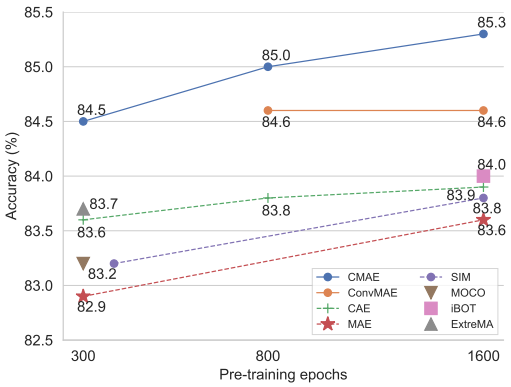

Figure 2: Comparisons with previous state-of-the-art MIM methods on ImageNet-1K in terms of top-1 accuracy at different pre-training epochs.

When we reflect on the success of MIM, it is inevitable to compare it with another well-proven and prevailing SSL method, i.e. contrastive learning (CL) [2, 35]. By adopting a simple discriminative idea that pulling closer representations from the same image and pushing away different images, CL methods naturally endow the pretained model with strong instance discriminability. In contrast to CL, MIM focuses more on learning local relations in input image for fulfilling the reconstruction task, instead of modeling the relation among different images [29]. Therefore, it is suspected that MIM is less efficient in learning discriminative representations. This issue has been manifested by experimental results in [25, 43]. Based on above analysis, it is thus natural to ask such a question: *can we leverage contrastive learning to further strengthen the representation learned by MIM methods?* or, in other words, *would MIM methods benefit from contrastive learning?* Along this direction, a few contemporary works attempt to train vision representation models [38, 51] by simply combining contrastive learning and MIM learning objectives. But they only show marginal performance gain compared to MIM methods. These results signify that it is non-trivial to fully leverage the advantages of both frameworks. The challenges are ascribed to various distinctions between them, including input augmentations, training objectives, model architectures, etc.

To overcome the challenges and learn better image representations for downstream tasks, we aim to explore a possible way to boost the MIM with contrastive learning in a unified framework. With a series of careful studies, we find that input view augmentation and latent feature alignment play important roles in harmonizing MIM and contrastive learning. We thus put dedicated efforts to these components to develop our method.

An overview of the proposed method is shown in Figure 1. More specifically, our method introduces a contrastive MAE (CMAE) framework for representation learning. It adopts a siamese architecture [5]. One branch is an online updated asymmetric encoder-decoder that learns latent representations to reconstruct masked images from a few visible patches, similar to MAE. The other branch is a momentum encoder that provides contrastive learning supervision. To leverage the contrastive learning to improve the feature quality of encoder output, we introduce an auxiliary feature decoder into the online branch, whose output features are used for contrastive learning with the momentum encoder outputs.

We carefully design each CMAE component to enable contrastive learning to benefit the MIM. Different from online encoder whose inputs only contain the visible patches, the CMAE momentum encoder is fed with the full set of image patches. This design ensures semantic integrity of its output features to guide the online encoder. Another notable design choice is: our method uses two decoders, one is to predict the image pixel and perform the MIM task; and another is to recover the features of masked tokens. Since the semantics of each patch are incomplete and ambiguous, it is problematic to use the features of patches directly for contrastive learning. Using an auxiliary feature decoder can address this issue and thus benefit the latent representation learning within the online branch. Moreover, different from existing methods that use strong spatial data augmentations for inputs, we propose a pixel shifting augmentation method for generating more plausible positive views

in contrastive learning. Such a simple augmentation is proven effective for improving MIM with contrastive learning.

With the above novel designs, the online encoder of our CMAE method can learn more discriminative features of holistic information and achieve state-of-the-art performance on various pre-training and transfer learning vision tasks.

Our contributions are summarized as follows. 1) We propose a new CMAE method to explore how to improve the representation of MIM by using contrastive learning. Its learned representations not only preserve the local context sensitive features but also model the instance discriminativeness among different images. 2) To impose contrastive learning upon MIM, we propose a feature decoder to complement the masked features and a weakly spatial shifting augmentation method for generating plausible contrastive views, both of which are effective in improving the encoder feature quality. 3) As shown in Figure 2, our method significantly improves the learned representation of MIM and sets new state-of-the-art performance. Notably, compared with prior arts, CMAE achieves absolute gains of 0.7% on ImageNet-1k classification validation split, 1.8% mIoU on ADE20K semantic segmentation validation dataset and 0.4% AP^b and 0.5% AP^m on CoCo validation split.

2 Related Work

Self-supervised learning is attracting increasing attention in computer vision. A bunch of methods have been proposed to advance this technique from different perspectives [4, 9, 18, 22, 25, 35, 47, 51]. Broadly speaking, these methods can be categorized into two groups depending on their employed pretext tasks, i.e., contrastive learning and mask image modeling.

Contrastive learning aims to learn instance discriminative representations to distinguish an image from the others. This is achieved by pulling together the representations of different views of an individual image and pushing away the other images. Thus, most contrastive methods adopt siamese network [10, 22, 24]. To create different views for the same image, a plentiful of data augmentation methods have been deployed (e.g., those investigated in SimCLR [9]). To better uitilize negative samples, MoCo [24] uses a large queue to cache negative examples in memory such that it can take in more negative examples for contrastive learning. BYOL [22] uses an online encoder to predict the output of a momentum encoder, where the momentum encoder is key to avoiding training collapse. To simplify BYOL, SimSiam [10] proposes the stop-gradient technique to replace the momentum updating. MoCo-v3 [11] and DINO [7] are based on the siamese network and extend MoCo [24] and BYOL [22] with Vision Transformer (ViT) as their model backbones. Although contrastive learning methods provide discriminative vision representations, most of them focus on learning global representations while lacking in the spatial-sensitive representation.

Mask image modeling [3, 8, 17] is inspired by the success of Masked Language Modeling in NLP [15] and learns vision representation by constructing the original signal from partial observations. Based on the reconstruction target, these methods can be devided into: pixel-domain reconstruction [18, 25, 40, 43] and auxiliary features/tokens prediction [3, 12, 16]. SimMIM [43] and MAE [25] propose to reconstruct the raw pixel values from either the full set of image patches (SimMIM) or partially observed patches (MAE) to reconstruct the raw image. Compared with SimMIM, MAE is more pre-training efficient because of masking out a large portion of input patches. To learn more semantic features, MaskFeat [40] introduces the low-level local features (HOG [13]) as the reconstruction target while CIM [18] opts for more complex input.

Several methods adopt an extra model to generate the target to pre-train the encoder. For instance, BEiT [3] uses the discretized tokens from an offline tokenizer [36] to train the encoder. PeCo [16] instead uses an offline visual vocabulary to guide the encoder. Differently, CAE [12] uses both the online target and offline network to guide the training of encoder. Furthermore, iBOT [51] introduces an online tokenizer to produce the target to distill the encoder. Similarly, SIM adopts the siamese network to reconstruct the representations of tokens, based on another masked view [38]. MSN [1] matches the representation of masked image to that of original image using a set of learnable prototypes.

Although MIM models have achieved promising performance, they focus on learning relations among the tokens in the input image, instead of modeling the relation among different images as contrastive learning, leading the learned representations to be less discriminative. Different from existing works,

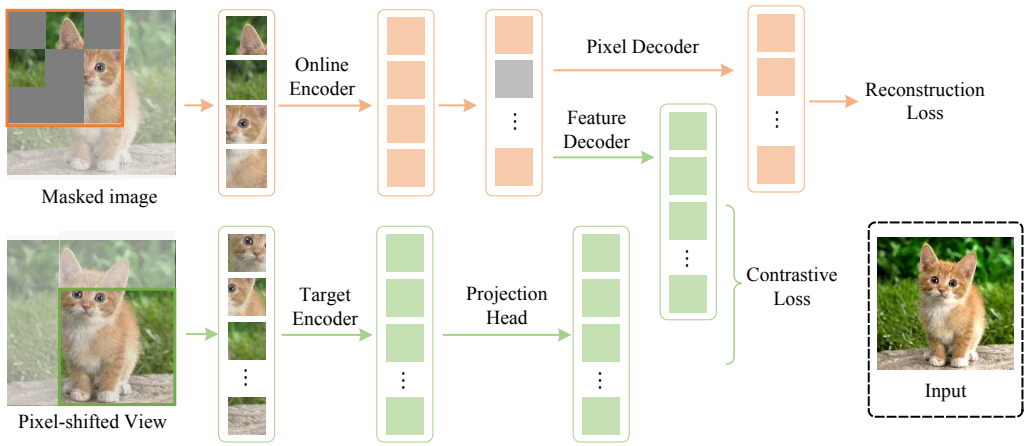

Figure 3: Overall pipeline. Our method contains three components: the online encoder, target encoder and online decoder. Given a training image, it applies *pixel shifting* to generate different views, which are then fed into the online and target encoders respectively. The online encoder randomly masks a fraction of the image patches and operates on the visible ones. The target encoder operates on the whole view after pixel shifting. The pixel decoder learns to reconstruct the input image from the image tokens (along with MASK tokens) provided by the online encoder, while the *feature decoder* learns to predict the features of the input image for contrastive learning with the target encoder output features. After the pre-training, only the online encoder is kept for downstream applications.

our method propose novel designs to fully exploit the advantages of MIM and contrastive learning, and thus it can provide local context sensitive representations with desired discriminativeness for input images.

3 Method

3.1 Framework

The overall framework of our method is illustrated in Figure 3 that consists of three components. The *online encoder and decoder* learn to reconstruct input images from masked observations. Different from existing MIM methods (e.g., MAE [25] and SimMIM [43]), our method further processes the input image via a spatially shifted cropping operation. More importantly, our decoder incorporates an additional feature decoder for predicting the input image features. The *target momentum encoder* transforms the augmented view of the input image into a feature embedding for contrastive learning with the predicted one from the online feature decoder. In this way, the learned representations by the online encoder capture not only holistic features of the input images but also discriminative features, thus achieving better generalization performance. We now elaborate on these components in detail.

In the following, we assume the input image I_s to the online encoder has been tokenized into a token sequence $\{x_i^s\}_{i=1}^N$ with N being the number of image patches (tokens). For its masked version, we denote the visible tokens as $\{x^v\}$. Similarly, the input tokens to the target encoder are denoted as $\{x_j^t\}_{j=1}^N$.

Online encoder The online encoder $\mathcal{F}_s$ maps the visible tokens x_s^v to embedding features z_s^v. Given the token sequence $\{x_i^s\}_{i=1}^N$, we mask out a large ratio of patches and feed the visited patches to the online encoder. The online encoder adopts the Vision Transformer (ViT) architecture [17], following MAE [25]. It first embeds the visible tokens x_s^v by linear projection as token embeddings, and adds the positional embeddings [39] p_s^v. We feed the fused embedding to a sequence of transformer blocks, and get the embedding features z_s^v.

$$z_s^v = \mathcal{F}_s(x_s^v + p_s^v) \tag{1}$$

After pre-training, the online encoder $\mathcal{F}_s$ is used for extracting image representations in downstream tasks.

Target encoder The target encoder is introduced for providing contrastive supervision for the online encoder to learn discriminative representations. Different from existing siamese-based methods [7, 51], our target encoder $\mathcal{F}_t$ only serves for contrastive learning, as well as guiding the online encoder to learn more discriminative features. It shares the same architecture as the online encoder $\mathcal{F}_s$, but takes the whole image as input, in order to reserve the semantic integrity and the discriminativeness of the learned representations. Using the whole image as input to the target encoder is important for the method performance, which is experimentally verified in Section 4.4. Unlike tokens in NLP, whose semantic are almost certain, image token is ambiguous in its semantic meaning [51]. To avoid ambiguity, we adopt global representations for contrastive learning. The mean-pooled feature of target encoder is used for its simplicity, i.e.

$$z_t = \frac{1}{N}\sum_{j=1}^{N}\mathcal{F}_t(x_j^t), \tag{2}$$

where x_j^t is the input token for target encoder and z_t is the representation of the input image.

Different from the online encoder, we update parameters of the target encoder by exponential moving average (EMA). That is, denoting the parameters of $\mathcal{F}_s$ and $\mathcal{F}_t$ as θ_s and θ_t respectively, the parameters are updated by $\theta_t \leftarrow \mu\theta_t + (1-\mu)\theta_s$. Here μ is fixed as 0.996 across the experiments. Momentum update is used since it stabilizes the training by fostering smooth feature changes, as found in MoCo [24] and BYOL [22].

Online decoder The decoder aims to map the latent features z_s^v and MASK token features to the feature space of the target encoder and the original images. Specifically, the decoder receives both the encoded visible tokens z_s^v and MASK tokens z_s^m.

Similar to MAE [25], position embeddings are added to input tokens. Due to different mapping targets, our online decoder has two branches of decoder structure, one is a pixel decoder, and another is a feature decoder. The pixel decoder $\mathcal{G}_p$ learns to reconstruct the pixel of the masked patches. We use the full set of tokens, which contains both z_s^v and z_s^m, to predict the pixel of patches y^m. This module can promote the model to learn holistic representation for each patch in an image. We set the pixel decoder to be stacked transformer blocks:

$$y'_m = \mathbb{I}\cdot\mathcal{G}_p(z_s^v, z_s^m), \tag{3}$$

where $\mathbb{I}$ is an indicator to only select the prediction corresponding to masked tokens, and y'_m is the output prediction for the masked patches.

To align with the output of the target encoder, feature decoder $\mathcal{G}_f$ is applied to recover the feature of masked tokens. The feature decoder has the same structure as the pixel decoder but non-shared parameters for serving a different learning target. The prominence of such design choices will be discussed in the architecture part in Section 3.4. Given the encoded visible tokens z_s^v, we add the masked tokens z_s^m and use this full set to predict the feature of masked tokens. Similar as done in target encoder, we apply the mean pooling operation on the output of feature decoder as the whole image representation y_s, and then use this feature for contrastive learning.

$$y_s = \frac{1}{N}\sum\mathcal{G}_f(z_s^v, z_s^m), \tag{4}$$

where N is the total number of tokens in the full set.

3.2 View augmentations

Typically, masking image modeling pre-training tasks only utilizes a single view of the input image, which only contains visited patches. But contrastive learning often adopts two different augmented views. To make MIM and contrastive learning be compatible with each other, our method also generates two different views and feeds them to its online and target branches, respectively.

In contrastive learning, the most commonly used view augmentations can be divided into two types: spatial transfer (e.g., random resized cropping, flipping) and color transfer (e.g., color jittering and random grayscaling). For MIM tasks, color enhancements degrade the results [25], so we do not apply them to the input of the online branch. Spatial and color data augmentations are applied to the target branch input to avoid a trivial solution.

We first consider two branches using two different random crops, following the common practice in contrastive learning. However, we observe this recipe has an adverse effect on model performance (refer to Section 4.4). We conjecture that this issue is related with the large disparity between the inputs of online/target encoders when randomly cropped regions are far apart or scarcely semantic-relevant. Different with using intact paired views in usual contrastive methods, the operation of masking out a large portion of input in MIM may amplify such disparity and therefore creates false positive views. Consequently, performing contrastive learning on these misaligned positive pairs actually incurs noise and hampers the learning of discriminative and meaningful representations.

To address the above issue, we propose a weakly augmentation method named **pixel shifting** for generating the inputs of online/target encoders. The core idea is first obtain a master image by a resized random cropping from the original image. Then two branches share the same master image and generate respective views by slightly shifting cropping locations over the master image. In more details, we denote the master image as I. The shape of I is $(w+p, h+p, 3)$, where w, h is the width and height of target input size for our model and p is the longest shifting range allowed. For online branch, we use the region of $[0:w, 0:h, :]$ as our input image I_s. For target branch, we use the region of $[r_w : r_w + w, r_h : r_h + h, :]$ as our input image I_t. r_w and r_h are independent random values in the range of $[0, p)$. Afterwards, image masking and color augmentation are still applied for I_s and I_t respectively.

3.3 Training Objective

Reconstruction loss Following [25], we use the normalized pixel as target in the reconstruction task. We adopt the Mean Squared Error (MSE) as loss function and compute the loss only on masked patches between the pixel decoder prediction and the original image. The math formulation is

$$L_r = \frac{1}{N_m} \sum (y'_m - y_m)^2, \tag{5}$$

where N_m is the number of masked patches in an image, and L_r is the loss value.

Contrastive loss For clarity, we describe the contrastive loss design of our method from two aspects: loss function and head structure. Two widely used loss functions are taken into consideration, i.e. InfoNCE [9, 24] loss and BYOL-style [7, 22] loss. The former seeks to simultaneously pull close positive views from the same sample and push away negative samples while the latter only maximizes the similarity between positive views. Although some recent works find they may be inherently unified [37], we still analyze them separately due to their diverse effects on representation learning. In our method, we observe better performance using InfoNCE [35] so we use it defaultly. Details are referred to Section 4.4. For the head structure, we adopt the widely used "projection-prediction" structure following [11, 22]. Specifically, we append the "projection-prediction" and "projection" head to feature decoder and target encoder respectively. The projection head with target encoder is also updated by exponential moving average. Due to the large differences on generating inputs for online/target encoder (refer to Section 3.2), we use asymmetric contrastive loss, which is distinguished from previous methods [11, 22]. The output of feature decoder y_s is transformed by the "projection-prediction" structure to get y_s^p. Similarly for the output of target encoder z_t, we apply the projection head and get z_t^p. We then compute the cosine similarity ρ between them:

$$\rho = \frac{y_s^p \cdot z_t^p}{\|y_s^p\|_2 \, \|z_t^p\|_2}. \tag{6}$$

We denote ρ^+ as the positive pairs cosine similarity, which is constructed by y_s^p and z_t^p from the same image. ρ_j^- indicates the cosine similarity for the j-th negative pair. We use the z_t^p from different images in a batch to construct negative pairs. The loss function of InfoNCE loss is

$$L_c = -\log \frac{\exp(\rho^+/\tau)}{\exp(\rho^+/\tau) + \sum_{j=1}^{K-1} (\exp(\rho_j^-/\tau))}, \tag{7}$$

where τ is the temperature constant, which is set to 0.07. K is the batch size.

The overall learning target is a weighted combination of reconstruction loss L_r and contrastive loss L_c defined as:

$$L = L_r + \lambda_c L_c. \tag{8}$$

	Training objective			Input	Architecture		Acc.
	recons. loss	intra-view match	intra-image contrast	pos. view alignment	feature complement	separate enc./dec.	
MSN [1]	✗	✓	✗	✗	✗	✗	83.4
ExtreMA [41]	✗	✓	✗	✓	✗	✗	83.7
MAE [25]	✓	✗	✗	N.A.	N.A.	✓	83.6
CAE [12]	✓	✗	✗	✗	✗	✓	83.9
iBot [51]	✓	✓	✗	✗	✗	✗	84.0
SIM [38]	✓	✓	✓	✗	✗	✓	83.8
CMAE	✓	✓	✓	✓	✓	✓	84.7

Table 1: Comparison of CMAE with previous methods on training objective, input generation and architecture. The top-1 accuracy on ImageNet is also presented. Please refer to Section 3.4 for more detailed explanations.

3.4 Connections and analysis

In order to better illustrate the connections and differences of CMAE with previous methods, we conduct comparisons among them from various aspects including training objective, input and architecture. The results are shown in Table 1. Particularly, we focus on those methods that either use contrastive information in MIM or masked image input. Methods using only MIM or contrastive learning are out of the scope of discussion since they are clearly distinguished from ours.

Training objective CMAE exploits both reconstruction loss and contrastive loss in optimization. As can be seen from Eq. (7), the contrastive loss used in CMAE involves both intra-view matching and intra-image contrast. Therefore, the learned representations are encouraged to have appealing properties of instance discriminability and spatial sensitivity. MSN and ExtreMA have different motivations with ours. They discard reconstruction loss and use masked input for the purpose of regularization or data augmentation. iBot only adopts a distillation loss between positive views by maximizing the intra-view matching scores, neglecting the contrastive learning with negative samples. Although SIM also employs both losses, it differs with CMAE on the reconstruction target. While CMAE recovers the masked content of the same view, SIM reconstructs the features of another view. We empirically show that our method is not only simpler but also more effective on representation learning by achieving higher performance.

Input Most previous methods for contrastive learning [9, 24] apply strong augmentation methods (e.g., random crop, random scale) to generate positive views from the same image. However, since the masking operation which employs a large masking ratio (e.g. 75% in [25]) already severely degrade the input, applying these augmentations on top may produce invalid positive views and thus hamper contrastive learning. In contrast, we propose a novel moderate data augmentation named pixel shifting for achieving better alignment between positive views. Compared to ExtreMA which uses exactly the same view in two siamese branches, pixel shifting is more flexible by introducing moderate input variance which turns out to be beneficial for contrastive learning (refer to Table 4a).

Architecture In CMAE, a lightweight feature decoder is added after the online encoder to complement the masked features. This is a prominent difference from other methods, e.g. SIM and iBot, which directly use the representations of the visible patches to match that of unmasked view. We argue that it is unreasonable to conduct contrastive learning between the features of the masked parts and the input images since they have distinct levels of abstractness and semantic coverage. Feature decoder is expected to benefit optimization by reducing such a distribution gap between contrastive features. The advantage of feature decoder is experimentally verified as shown in Table 4c.

4 Experiments

4.1 Implementation Details

Pre-training. We follow the settings of MAE [25] to pre-train our model. We adopt AdamW [33] optimizer as default, and the momentum is set to $\beta_1 = 0.9$, $\beta_2 = 0.95$. Besides, the weight decay is

Method	Pre-training epochs	Params.(M)	Supervision	Accuracy
MoCo-v3 [11]	300	86	RGB	83.2
DINO [7]	300	86	RGB	82.8
CIM [18]	300	86	RGB	83.3
BEiT [3]	800	86	DALLE	83.2
SimMIM [43]	800	86	RGB	83.8
PeCo [16]	800	86	Perceptual Codebook	84.5
MaskFeat [40]	1600	86	HOG	84.0
CAE [12]	1600	86	DALLE+RGB	83.9
iBOT [51]	1600	86	RGB	84.0
SIM [38]	1600	86	RGB	83.8
MAE [25]	1600	86	RGB	83.6
CMAE (ours)	800	86	RGB	84.4
CMAE (ours)	1600	86	RGB	**84.7**
ConvMAE* [19]	800	86	RGB	84.6
ConvMAE* [19]	1600	86	RGB	84.6
CMAE* (ours)	800	86	RGB	85.0
CMAE* (ours)	1600	86	RGB	**85.3**

Table 2: Comparison of our model with existing methods on ViT-B. We evaluate them with the top-1 accuracy on ImageNet. The symbol of * throughout experiments denotes using convolutions instead of linear transformation as the tokenizer for visual patches.

set to 0.05. We use the linear scaling rule [21]: $lr = base_lr \times batch_size/256$ to set the learning rate. The base learning rate is 1.5×10^{-4} with a batch size of 4096. Cosine learning rate schedule [32] with a warmup of 40 epochs is adopted. All pre-training experiments are conducted on 32 NVIDIA A100 GPUs.

Encoder Structure. We use the ViT [17] base model as our default setting. To further validate the extensibility of our proposed model, we replace the ViT with a hybrid convolutional ViT which is also used by ConvMAE [19]. In the hybrid ViT, a multi-layer convolutional network [28] is used as token projection. Note the hybrid ViT is made to have the same model size as the ViT counterpart for fair comparison. We also experiment with scaled up encoders for evaluating the scalability of our method.

4.2 Results on ImageNet

Following existing works [3, 11, 25, 43], we use ImageNet-1K [14] which consists of 1.3M images of 1k categories as the pre-training and fine-tuning dataset. The dataset contains two subsets: the training set and the validation set. We only use the training set to pre-train CMAE. After pre-training, the CMAE online encoder is used for fine-tuning on ImageNet-1k training set for 100 epochs. For the model pre-trained with 300 epochs, we adopt $5.e^{-4}$ as the base learning rate in fine-tuning. Since the longer pre-training schedule (1600 epochs) makes the model learn better initialization weights for fine-tuning [44], we set a smaller base learning rate of $2.5e^{-4}$. Besides, we follow the common fine-tuning practices to regularize the model using mixup [48], cutmix [46], drop path [27], etc.

In Table 2, we compare CMAE with competing methods on the fine-tuning classification accuracy on ImageNet. CMAE achieves a top-1 accuracy of 84.7%, which is 1.1% higher than MAE [25]. Among all models using ViT architecture, CMAE achieves the best performance. Compared with contrastive learning based methods Moco-v3 [11] and DINO [7], our model can significantly outperform them by 1.5% and 1.9% respectively. Compared with iBOT and SIM which also use contrastive objective in MIM, our CMAE achieves higher performance with a gain of 0.7% and 0.8%, respectively. Above results strongly evidence the superiority of CMAE.

When we replace the vanilla ViT encoder with a hybrid convolutional ViT, as done in ConvMAE [19], CMAE further improves to 85.0% and 85.3% with the pre-training of 800 epochs and 1600 epochs, respectively. These results surpass those of ConvMAE under the same pre-training setting by 0.4% and 0.7% respectively, verifying the excellent extendibility of CMAE to various network structures.

Method	Pre-Epochs	mIoU
MoCo-v3 [11]	300	47.3
DINO [7]	400	47.2
BEiT [3]	800	47.1
CIM [18]	300	43.5
CAE [12]	1600	50.2
iBOT [51]	1600	50.0
PeCo [16]	800	48.5
MAE [25]	1600	48.1
CMAE	1600	**51.0**
ConvMAE* [19]	1600	50.7
CMAE*	1600	**52.5**

(a) Semantic segmentation results on ADE20K. We use UperNet as our default segmentation framework.

Method	Pre-Epochs	AP^{bbox}	AP^{mask}
MoCo-v3 [11]	300	47.9	42.7
BEiT [3]	800	49.8	44.4
CAE [12]	1600	50.0	44.0
iBOT‡ [51]	1600	51.2	44.2
PeCo [16]	800	44.9	40.4
SIM [38]	1600	49.1	43.8
MAE† [25]	1600	51.7	45.9
MAE [25]	1600	50.3	44.9
CMAE	1600	**52.4**	**46.5**
ConvMAE* [19]	1600	52.5	46.5
CMAE*	1600	**52.9**	**47.0**

(b) COCO object detection and segmentation. We use the Mask R-CNN model [23] as our framework. ‡ means using Cascade Mask R-CNN [6].

Table 3: Performance comparison on downstream tasks, including semantic segmentation and object detection. The symbol of * denotes using convolutions to embed visual patches. † denotes reproduced results of ours.

Remarkably, CMAE can gain a noticeable improvement with a prolonged training schedule (from 800 epochs to 1600 epochs) while ConvMAE is observed to saturate at 800 epochs. This result suggests the stronger capability of CMAE on learning better representations.

4.3 Transfer Learning

To further validate the transferability of CMAE, we follow previous methods to evaluate pre-trained models on the semantic segmentation dataset ADE20K [50] and the object detection dataset COCO2017 [31].

Semantic segmentation. ADE20K [50] has 25,562 images of 150 fine-grained categories. We adopt Upernet [42] as the default model for this task, following the settings of compared methods. The backbone ViT-B is initialized from pre-training while other modules are initialized with the Xavier [20] initialization. The model is fine-tuned on the training set of ADE20K and tested on standard validation split.

Following previous works, we report the Mean Intersection over Union (mIoU) performance of CMAE in Table 3a. We notice that CMAE significantly surpasses MAE by 2.9%, which verifies the stronger transferability of CMAE. Besides, CMAE also improve by 1.0% and 0.8% compared with iBOT [51] and CAE [12] respectively. With the same hybrid ViT backbone, CMAE significantly outperforms ConvMAE by 1.8%. Remarkably, CMAE sets a new state-of-the-art result of 52.5 by surpassing all competing methods with a large margin.

Object Detection and Segmentation. We adopt the widely used object detection and instance segmentation framework Mask-RCNN [23, 30] for benchmarking on this task. ViT-B is used as the backbone and initialized with our pre-trained model. Following MAE, we fine-tune the model on COCO train2017 split, and report box AP for object detection and mask AP for instance segmentation on val2017 split. We fine-tune the model for 100 epochs. The base learning rate is $1.e^{-4}$ with a cosine annealing schedule, and the weight decay is set to 0.1.

The comparison results with other self-supervised learning methods are shown in Table 3b. As one can see, CMAE improves over MAE from 51.7 to 52.4 on AP^b and from 45.9 to 46.5 on AP^m. With the hybrid ViT structure, CMAE consistently surpasses the competing method ConvMAE: AP^b increases from 52.5 to 52.9 and AP^m increases from 46.5 to 47.0. Above promising results again verify the effectiveness of our method.

Setting	Accuracy
Baseline [25]	82.9
+ Contrastive learning	83.1
+ Pixel shifting aug.	83.6
+ Feature decoder	83.8

(a) Component analysis.

Rand crop	Pixel shift	Color Aug.	Accuracy
✗	✗	✗	82.9
✓	✗	✗	83.0
✗	✓	✗	83.4
✗	✓	✓	83.8

(b) Data augmentation analysis.

#Blocks	Share weight	Accuracy
0	✗	83.6
2	✗	83.8
2	✓	83.4
4	✗	83.8
4	✓	83.5

(c) Feature decoder analysis.

Loss weight	Accuracy
0.1	83.3
0.5	83.7
1.0	83.8
1.5	83.5
2.0	83.2

(d) Contrastive loss weight.

Masking ratio	Accuracy
0	83.8
0.25	83.6
0.5	83.3
0.65	83.3
0.75	83.0

(e) Target encoder masking ratio.

Table 4: Ablations. We evaluate all the results on ImageNet-1k with top-1 accuracy. We initialize the model with the weights after 300-epoch pretraining.

4.4 Method Analysis

To understand the effects of key components and validate design choices we adopt in CMAE, we conduct a series of ablation experiments. Unless otherwise stated, we report the performance of our model with 300 pre-training epochs in this subsection. The ablative results are listed in Table 4. In the following, we verify the effectiveness of our main design ideas, then conduct ablation experiments for each component separately.

Ablation of components In Table 4a, we show how each component, i.e. contrastive learning, pixel shifting data augmentation and feature decoder affects model's performance. We start with a vanilla implementation of contrastive learning on MAE. Specifically, following the input generation approach in contrastive methods, random cropped regions with masking are fed into online/target encoder. The same contrastive objective as introduced in Section 3.3 are optimized between the output of online encoder and target encoder. As can be seen from Table 4a, such an intuitive approach only leads to marginal improvement (0.2%). Apparently, the power of contrastive learning is not fully unleashed due to ignoring its compatibility with MIM. By using the proposed moderate data augmentation, i.e. pixel shifting, the result can increase from 83.1% to 83.6%, which evidences the advantage of pixel shifting. Moreover, applying feature decoder further boosts the model's learning capability by improving the performance to 83.8%, demonstrating its effectiveness in our method.

Contrastive loss To explore the effect of contrastive loss in CMAE, we experiment with various loss weights, i.e. λ_c in Eq. (8). The results are shown in Table 4d. Note CMAE degenerates to the baseline MAE when loss weight is 0. When increasing the weights from 0 to 1, the model's performance increases accordingly, which verifies the importance of contrastive learning on enhancing the learned representations. When the weight of contrast learning is greater than that of MIM, we observe the phenomenon of imbalanced training occurs which adversely affects the final performance. This experiment demonstrates that both contrastive loss and reconstructive loss are critical for learning capable representations. We therefore set $\lambda_c = 1$ throughout our experiments.

We also conduct controlled experiments with different contrastive loss forms to compare their influences on pre-training. Under the same configuration, we observe that the model trained with InfoNCE loss achieves higher performance than BYOL-style loss (83.8% vs. 83.4%). This result suggests that the way of utilizing negative samples in InfoNCE is more effective in our method.

Pixel shifting augmentation In this section, we ablate on the importance of data augmentations. In contrast to the common practices of applying heavy data augmentation in contrastive learning, we find a moderate data augmentation is more effective in aligning contrastive learning and MIM. We divide data augmentation methods into two kinds: spatial transfer and color transfer, and evaluate their effect respectively. For spatial transfer, we compare our proposed pixel shifting with the commonly used

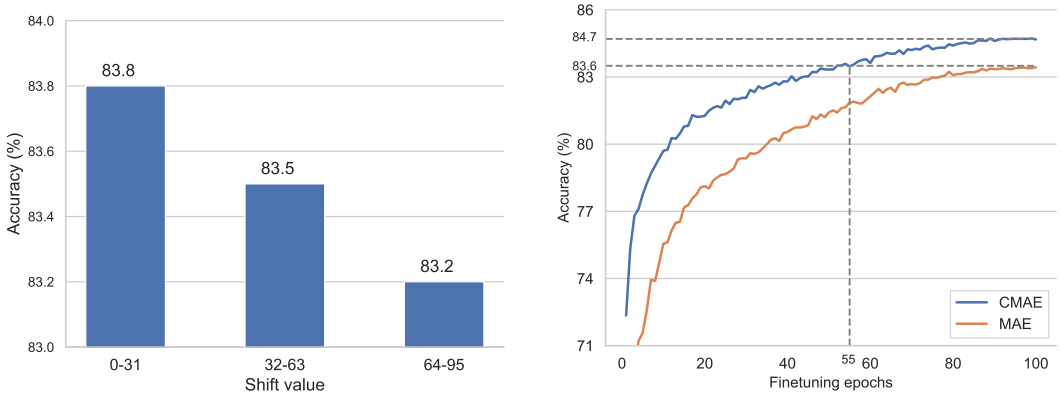

(a) Impact of different pixel shift ranges.

(b) Convergence speed compared with MAE.

Figure 4: Model performance with different settings of pixel shift and training epochs on ImageNet-1k.

randomly resized cropping. For color transfer, we compare two cases, i.e. with or without using color jittering for the target branch.

As can be seen from Table 4b, pixel shifting significantly surpasses random crop (83.4% vs. 83.0%). The superiority of pixel shifting should be attributed to its ability of generating more plausible positive views. As introduced in Section 3.2, this property helps contrastive learning better collaborate with MIM in our framework. By using color transfer, the result further improves to 83.8%, suggesting color transfer is complementary to our method.

We further study different settings of pixel shifting by varying shift ranges. Intuitively, larger shifts leads to greater differences between two views. As one can observe from Figure 4a, too large shifts severely degrades the model performance which comply with our assumption that misaligned positive views may bring noise to contrastive learning. Based on above results, we choose the shift range of $[0, 31)$ as default setting.

Feature decoder Different from existing works, we introduce a feature decoder to recover the features of masked patches when performing contrastive learning. To investigate its effectiveness, we present experiments under following two settings: sharing the weight between feature decoder and pixel decoder or not, and changing the depth of feature decoder.

In Table 4c, number "0" means not using feature decoder, i.e. the output of the online encoder which contains only the features of visible tokens is used for contrastive learning. Under this setting, our method performs worse than using a lightweight two-layer feature decoder. When increasing the depth of feature decoder, there is no significant impact on performance. However, when the depth increases to 8, we obtain a trivial solution, possibly due to the optimization difficulty caused by deeper structure. To strike a balance between efficiency and effectiveness, we set the depth to be 2. Besides, when the feature decoder shares the weight with the pixel decoder, the method performs the worst. A plausible explanation is that the two branches have different targets, thus should adopt independent weights.

Masking ratio for the target branch In this experiment, we investigate whether masking a portion of image patches for the target branch affects the model performance. Following previous works, we select a set of masking ratios, including $\{0, 0.25, 0.5, 0.65, 0.75\}$ for the target branch and see how the performance changes. As shown in Table 4e, one can observe that using the complete set of the image tokens yields the best results. A possible reason is that: since the aim of adding the target branch is to provide our model with the contrastive supervision, incorporating the full semantics of an image is preferred. Otherwise, the masked input with degenerated semantic information may lead to a sub-optimal solution in contrastive learning. Based on this observation, the target branch in our model uses the whole image as input throughout our experiments.

Convergence speed To further show our method's effectiveness, we compare the convergence behavior of CMAE and MAE when fine-tuning on ImageNet-1k. The pre-trained weights with 1600

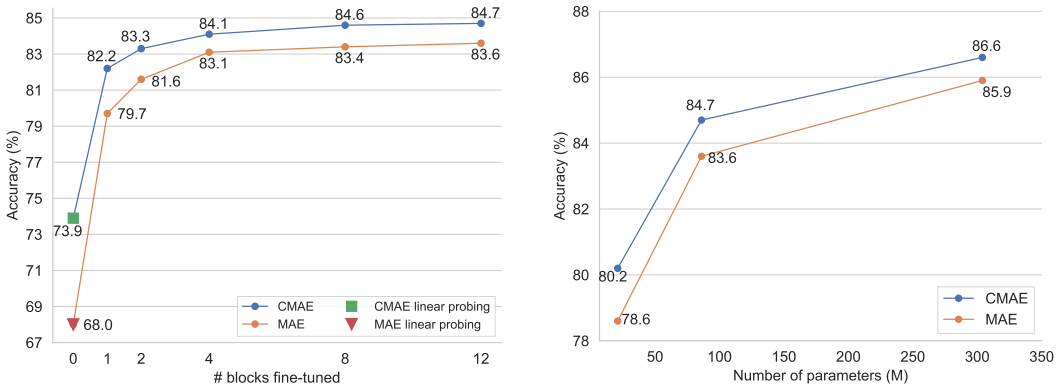

(a) Partial fine-tuning results of ViT-B.

(b) Results with different model size.

Figure 5: Performance comparison on ImageNet-1k with partial fine-tuning and model scaling. Partial fine-tuning adopts the model with weights that are pre-trained with 1600 epochs. For model scaling experiments, all models are pre-trained with 1600 epochs.

epochs are used as initialization. As shown in Figure 4b, we observe that CMAE converges much faster compared with MAE: with only 55 fine-tuning epochs, CMAE already surpasses the final performance of MAE. This result demonstrates that the representations learned by CMAE can be more easily adapted for specific tasks, an appealing property which is in line with the purposes of self-supervised pre-training.

4.5 Partial Fine-tuning and Linear Probing

In addition to fine-tuning whole model, partial fine-tuning [25, 34, 45, 49] and linear probing are also used to evaluate the quality of learned representation in self-supervised methods. Both partial fine-tuning and linear probing freeze most parts of the model when trained on specific tasks. They differ in that the former tunes a non-linear head while the former tunes a linear one. As indicated by [25], since linear probing is largely uncorrelated with transfer learning performance, partial fine-tuning is a better protocol for evaluating non-linear yet stronger representations. Based on the above observations, we also focus on the partial fine-tuning metric.

Specifically, we follow the experimental settings of [25] to ablate the CMAE base model with 1600 epoch pre-training. As shown in Figure 5a, the performances of our model are consistently better than MAE in all tested settings, e.g. when fine-tuning one block, we get a 2.5% gain over MAE. Above results demonstrate that our model can effectively improve the representation quality of baseline method. Note when the number of fine-tuned blocks is "0", it degenerates to linear probing. In this case, our model achieves significant improvement (5.9%) over MAE. These results indicate that our method is able to improve the representation quality under both evaluation metrics.

4.6 Model Scaling

To study the scalability of our method for models of different sizes, we adopt ViT-small, ViT-base, and ViT-large as encoders and report their performance on ImageNet-1k fine-tuning. As shown in Figure 5b, CMAE can consistently boost the performance of MAE at all scales. These results clearly demonstrate the excellent scalability of CMAE.

5 Conclusion

This paper introduces a novel self-supervised learning framework named contrastive masked autoencoder (CMAE) which aims to improve the representation quality of MIM by leveraging contrastive learning. In CMAE, we propose two novel designs from the perspective of input generation and architectures respectively to harmonize MIM and contrastive learning. Through extensive experiments, it is demonstrated that CMAE can significantly improve the quality of learned representation in pre-training. Notably, on three well-established downstream tasks, i.e. image classification/segmentation/detection, CMAE achieves state-of-the-art performance. In the future, we will investigate the scaling up of CMAE to larger dataset.

References

[1] M. Assran, M. Caron, I. Misra, P. Bojanowski, F. Bordes, P. Vincent, A. Joulin, M. Rabbat, and N. Ballas. Masked siamese networks for label-efficient learning. *arXiv preprint arXiv:2204.07141*, 2022.

[2] P. Bachman, R. D. Hjelm, and W. Buchwalter. Learning representations by maximizing mutual information across views. *NeurIPS*, 32, 2019.

[3] H. Bao, L. Dong, and F. Wei. Beit: Bert pre-training of image transformers. *arXiv preprint arXiv:2106.08254*, 2021.

[4] A. Bardes, J. Ponce, and Y. LeCun. Vicreg: Variance-invariance-covariance regularization for self-supervised learning. *arXiv preprint arXiv:2105.04906*, 2021.

[5] J. Bromley, I. Guyon, Y. LeCun, E. Säckinger, and R. Shah. Signature verification using a" siamese" time delay neural network. *Advances in Neural Information Processing Systems*, 6, 1993.

[6] Z. Cai and N. Vasconcelos. Cascade r-cnn: high quality object detection and instance segmentation. *TPAMI*, 43(5):1483–1498, 2019.

[7] M. Caron, H. Touvron, I. Misra, H. Jégou, J. Mairal, P. Bojanowski, and A. Joulin. Emerging properties in self-supervised vision transformers. In *ICCV*, pages 9650–9660. IEEE, 2021.

[8] M. Chen, A. Radford, R. Child, J. Wu, H. Jun, D. Luan, and I. Sutskever. Generative pretraining from pixels. In *ICML*, pages 1691–1703. PMLR, 2020.

[9] T. Chen, S. Kornblith, M. Norouzi, and G. Hinton. A simple framework for contrastive learning of visual representations. In *ICML*, pages 1597–1607. PMLR, 2020.

[10] X. Chen and K. He. Exploring simple siamese representation learning. In *CVPR*, pages 15750–15758. IEEE, 2021.

[11] X. Chen, S. Xie, and K. He. An empirical study of training self-supervised vision transformers. In *ICCV*, pages 9640–9649. IEEE, 2021.

[12] X. Chen, M. Ding, X. Wang, Y. Xin, S. Mo, Y. Wang, S. Han, P. Luo, G. Zeng, and J. Wang. Context autoencoder for self-supervised representation learning. *arXiv preprint arXiv:2202.03026*, 2022.

[13] N. Dalal and B. Triggs. Histograms of oriented gradients for human detection. In *CVPR*, volume 1, pages 886–893. IEEE, 2005.

[14] J. Deng, W. Dong, R. Socher, L.-J. Li, K. Li, and L. Fei-Fei. Imagenet: A large-scale hierarchical image database. In *CVPR*, pages 248–255. IEEE, 2009.

[15] J. Devlin, M.-W. Chang, K. Lee, and K. Toutanova. Bert: Pre-training of deep bidirectional transformers for language understanding. *arXiv preprint arXiv:1810.04805*, 2018.

[16] X. Dong, J. Bao, T. Zhang, D. Chen, W. Zhang, L. Yuan, D. Chen, F. Wen, and N. Yu. Peco: Perceptual codebook for bert pre-training of vision transformers. *arXiv preprint arXiv:2111.12710*, 2021.

[17] A. Dosovitskiy, L. Beyer, A. Kolesnikov, D. Weissenborn, X. Zhai, T. Unterthiner, M. Dehghani, M. Minderer, G. Heigold, S. Gelly, et al. An image is worth 16x16 words: Transformers for image recognition at scale. *arXiv preprint arXiv:2010.11929*, 2020.

[18] Y. Fang, L. Dong, H. Bao, X. Wang, and F. Wei. Corrupted image modeling for self-supervised visual pre-training. *arXiv preprint arXiv:2202.03382*, 2022.

[19] P. Gao, T. Ma, H. Li, J. Dai, and Y. Qiao. Convmae: Masked convolution meets masked autoencoders. *arXiv preprint arXiv:2205.03892*, 2022.

[20] X. Glorot and Y. Bengio. Understanding the difficulty of training deep feedforward neural networks. In *AISTATS*, pages 249–256. JMLR Workshop and Conference Proceedings, 2010.

[21] P. Goyal, P. Dollár, R. Girshick, P. Noordhuis, L. Wesolowski, A. Kyrola, A. Tulloch, Y. Jia, and K. He. Accurate, large minibatch sgd: Training imagenet in 1 hour. *arXiv preprint arXiv:1706.02677*, 2017.

[22] J.-B. Grill, F. Strub, F. Altché, C. Tallec, P. Richemond, E. Buchatskaya, C. Doersch, B. Avila Pires, Z. Guo, M. Gheshlaghi Azar, et al. Bootstrap your own latent-a new approach to self-supervised learning. In *NeurIPS*, volume 33, pages 21271–21284, 2020.

[23] K. He, G. Gkioxari, P. Dollár, and R. Girshick. Mask r-cnn. In *ICCV*, pages 2961–2969. IEEE, 2017.

[24] K. He, H. Fan, Y. Wu, S. Xie, and R. Girshick. Momentum contrast for unsupervised visual representation learning. In *CVPR*, pages 9729–9738. IEEE, 2020.

[25] K. He, X. Chen, S. Xie, Y. Li, P. Dollár, and R. Girshick. Masked autoencoders are scalable vision learners. In *CVPR*, pages 16000–16009. IEEE, 2022.

[26] G. E. Hinton and R. Zemel. Autoencoders, minimum description length and helmholtz free energy. *NeurIPS*, 6, 1993.

[27] G. Huang, Y. Sun, Z. Liu, D. Sedra, and K. Q. Weinberger. Deep networks with stochastic depth. In *ECCV*, pages 646–661. Springer, 2016.

[28] Y. LeCun, B. Boser, J. S. Denker, D. Henderson, R. E. Howard, W. Hubbard, and L. D. Jackel. Backpropagation applied to handwritten zip code recognition. *Neural computation*, 1(4): 541–551, 1989.

[29] S. Li, D. Wu, F. Wu, Z. Zang, K. Wang, L. Shang, B. Sun, H. Li, S. Li, et al. Architecture-agnostic masked image modeling–from vit back to cnn. *arXiv preprint arXiv:2205.13943*, 2022.

[30] Y. Li, S. Xie, X. Chen, P. Dollar, K. He, and R. Girshick. Benchmarking detection transfer learning with vision transformers. *arXiv preprint arXiv:2111.11429*, 2021.

[31] T.-Y. Lin, M. Maire, S. Belongie, J. Hays, P. Perona, D. Ramanan, P. Dollár, and C. L. Zitnick. Microsoft coco: Common objects in context. In *ECCV*, pages 740–755. Springer, 2014.

[32] I. Loshchilov and F. Hutter. Sgdr: Stochastic gradient descent with warm restarts. *ICLR*, 2017.

[33] I. Loshchilov and F. Hutter. Decoupled weight decay regularization. *arXiv preprint arXiv:1711.05101*, 2017.

[34] M. Noroozi and P. Favaro. Unsupervised learning of visual representations by solving jigsaw puzzles. In *ECCV*, pages 69–84. Springer, 2016.

[35] A. v. d. Oord, Y. Li, and O. Vinyals. Representation learning with contrastive predictive coding. *arXiv preprint arXiv:1807.03748*, 2018.

[36] A. Ramesh, M. Pavlov, G. Goh, S. Gray, C. Voss, A. Radford, M. Chen, and I. Sutskever. Zero-shot text-to-image generation. In *ICML*, pages 8821–8831. PMLR, 2021.

[37] C. Tao, H. Wang, X. Zhu, J. Dong, S. Song, G. Huang, and J. Dai. Exploring the equivalence of siamese self-supervised learning via a unified gradient framework. In *CVPR*, pages 14431–14440. IEEE, 2022.

[38] C. Tao, X. Zhu, G. Huang, Y. Qiao, X. Wang, and J. Dai. Siamese image modeling for self-supervised vision representation learning. *arXiv preprint arXiv:2206.01204*, 2022.

[39] A. Vaswani, N. Shazeer, N. Parmar, J. Uszkoreit, L. Jones, A. N. Gomez, Ł. Kaiser, and I. Polosukhin. Attention is all you need. *NeurIPS*, 30, 2017.

[40] C. Wei, H. Fan, S. Xie, C.-Y. Wu, A. Yuille, and C. Feichtenhofer. Masked feature prediction for self-supervised visual pre-training. In *CVPR*, pages 14668–14678. IEEE, 2022.

[41] Z. Wu, Z. Lai, X. Sun, and S. Lin. Extreme masking for learning instance and distributed visual representations. *arXiv preprint arXiv:2206.04667*, 2022.

[42] T. Xiao, Y. Liu, B. Zhou, Y. Jiang, and J. Sun. Unified perceptual parsing for scene understanding. In *ECCV*, pages 418–434. Springer, 2018.

[43] Z. Xie, Z. Zhang, Y. Cao, Y. Lin, J. Bao, Z. Yao, Q. Dai, and H. Hu. Simmim: A simple framework for masked image modeling. In *CVPR*, pages 9653–9663. IEEE, 2022.

[44] Z. Xie, Z. Zhang, Y. Cao, Y. Lin, Y. Wei, Q. Dai, and H. Hu. On data scaling in masked image modeling. *arXiv preprint arXiv:2206.04664*, 2022.

[45] J. Yosinski, J. Clune, Y. Bengio, and H. Lipson. How transferable are features in deep neural networks? *NeurIPS*, 27, 2014.

[46] S. Yun, D. Han, S. J. Oh, S. Chun, J. Choe, and Y. Yoo. Cutmix: Regularization strategy to train strong classifiers with localizable features. In *ICCV*, pages 6023–6032. IEEE, 2019.

[47] J. Zbontar, L. Jing, I. Misra, Y. LeCun, and S. Deny. Barlow twins: Self-supervised learning via redundancy reduction. In *ICML*, pages 12310–12320. PMLR, 2021.

[48] H. Zhang, M. Cisse, Y. N. Dauphin, and D. Lopez-Paz. mixup: Beyond empirical risk minimization. In *ICLR*, 2018.

[49] R. Zhang, P. Isola, and A. A. Efros. Colorful image colorization. In *ECCV*, pages 649–666. Springer, 2016.

[50] B. Zhou, H. Zhao, X. Puig, T. Xiao, S. Fidler, A. Barriuso, and A. Torralba. Semantic understanding of scenes through the ade20k dataset. *IJCV*, 127(3):302–321, 2019.

[51] J. Zhou, C. Wei, H. Wang, W. Shen, C. Xie, A. Yuille, and T. Kong. ibot: Image bert pre-training with online tokenizer. *ICLR*, 2022.